Free-Energy and Structural Analysis of Ion Solvation and Contact Ion-Pair Formation of Li+ with BF4- and PF6- in Water and Carbonate Solvents

ARTICLE *in* THE JOURNAL OF PHYSICAL CHEMISTRY B · MAY 2012

Impact Factor: 3.3 · DOI: 10.1021/jp3011487 · Source: PubMed

6 AUTHORS, INCLUDING:

Yasuo Kameda
Yamagata University
131 PUBLICATIONS **1,390** CITATIONS
SEE PROFILE

Babak Minofar
Center for Nanobiology and Structural Biology…
30 PUBLICATIONS **588** CITATIONS
SEE PROFILE

Yasuhiro Umebayashi
Niigata University
115 PUBLICATIONS **2,252** CITATIONS
SEE PROFILE

THE JOURNAL OF PHYSICAL CHEMISTRY B

Article

pubs.acs.org/JPCB

Free-Energy and Structural Analysis of Ion Solvation and Contact Ion-Pair Formation of Li^+ with BF_4^- and PF_6^- in Water and Carbonate Solvents

Munetaka Takeuchi,[‡] Nobuyuki Matubayasi,*[,§,⊥] Yasuo Kameda,[∥] Babak Minofar,[‡] Shin-ichi Ishiguro,[‡] and Yasuhiro Umebayashi*[,‡,†]

[‡]Department of Chemistry, Faculty of Science, Kyushu University, Fukuoka 812-8581, Japan

[§]Institute for Chemical Research, Kyoto University, Uji, Kyoto 611-0011, Japan

[⊥]Japan Science and Technology Agency (JST), CREST, Kawaguchi, Saitama 332-0012, Japan

[∥]Department of Material and Biological Chemistry, Faculty of Science, Yamagata University, Yamagata 990-8560, Japan

ABSTRACT: Free energy of contact ion-pair (CIP) formation of lithium ion with BF_4^- and PF_6^- in water, propylene carbonate (PC), dimethyl carbonate (DMC) are quantitatively analyzed using MD simulations combined with the energy representation method. The relative stabilities of the mono-, bi-, and tridentate coordination structures are assessed with and without solvent, and water, PC, and DMC are found to favor the CIP−solvent contact. The monodentate structure is typically most stable in these solvents, whereas the configuration is multidentate in vacuum. The free energy of CIP formation is not simply governed by the solvent dielectric constant, and microscopic analyses of solute−solvent interaction at a molecular level are then performed from energetic and structural viewpoints. Vacant sites of Li^+ cation in CIP are solvated with three carbonyl oxygen atoms of PC and DMC solvent molecules, and the solvation is stronger for the monodentate CIP than for the multidentate. Energetically favorable solute−solvent configurations are shown to be spatially more restricted for the multidentate CIP, leading to the observation that the solvent favors the monodentate coordination structure.

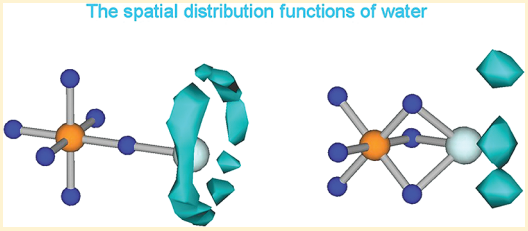

1. INTRODUCTION

Having the smallest ionic radius among monovalent metal cations, lithium ion is distinct in its structure and dynamics in solutions.[1−5] While the coordination number of the lithium ion is well accepted to be four in water, it is still a target of active investigations. For example, neutron/X-ray diffraction experiments have revealed that the coordination number varies from four to six, depending on the salt concentration and counteranion species.[6] The lithium ion dynamics cannot further be described by the classical Stokes−Einstein law,[7] and a new molecular approach is being sought.

On the standpoint of electrochemistry and related industries, lithium has the most negative redox potential among all elements (Li/Li^+ = −3.06 V (vs NHE)), hence the lithium secondary battery is one of the most expected electric storages due to its high energy density.[8,9] In designing batteries, nonaqueous solvents of carbonates are often used, for instance, propylene carbonate (PC), ethylene carbonate (EC), and dimethyl carbonate (DMC)[10,11] and also their mixtures owing to their availability as a liquids in a wide temperature range, chemical and electrical stability, large lithium ion solubility, and low toxicity.[12] Contact ion-pair (CIP) formation ability of electrolyte in a lithium battery plays an important role in the lithium ion conduction. To increase the conductivity of the lithium ion, it is required to keep the single-ion concentration and prevent the CIP formation. Favorable anions are thus of weak coordination nature such as BF_4^- or PF_6^-. A molecular study of lithium solvation and CIP formation is thus not only interesting for their physical and chemical properties but also useful for designing a lithium salt for a high performance battery.

The CIP formation has been studied by a number of experimental techniques such as static[13] and dynamic[14,15] ionic conductivity, Raman/IR[16−24] and NMR.[25] Sano et al. have investigated the $LiPF_6$[26] and $LiBF_4$[27] in PC solutions in terms of ionic conductivity, solution viscosity, and self-diffusion coefficient over the wide rang of salt concentration, and revealed that the higher conductivity of $LiPF_6$ in dilute solutions is related to the weaker CIP formation ability of the PF_6^-. The CIP stability is closely related to the CIP structure. Structural study on the lithium ion in highly concentrated $LiPF_6$/PC solution has been performed by means of neutron diffraction experiments with $^{6/7}$Li isotopic substitution technique.[28] Also some theoretical studies about CIP have been reported.[29−32] Borodin and Smith carried out MD simulations of $LiBF_6$ in EC:DMC mixed solvents with many-body polarizable force fields.[33] In fact, there are a few candidates for the CIP structure (Chart 1), and the structure

Received: February 4, 2012
Revised: May 1, 2012
Published: May 22, 2012

   dx.doi.org/10.1021/jp3011487 | J. Phys. Chem. B 2012, 116, 6476−6487

Chart 1. Molecular Geometries and Atomic Charges of the Ion-Pairs of $LiBF_4$ and $LiPF_6$ and the solvent molecules of PC, DMC, and H_2O[a]

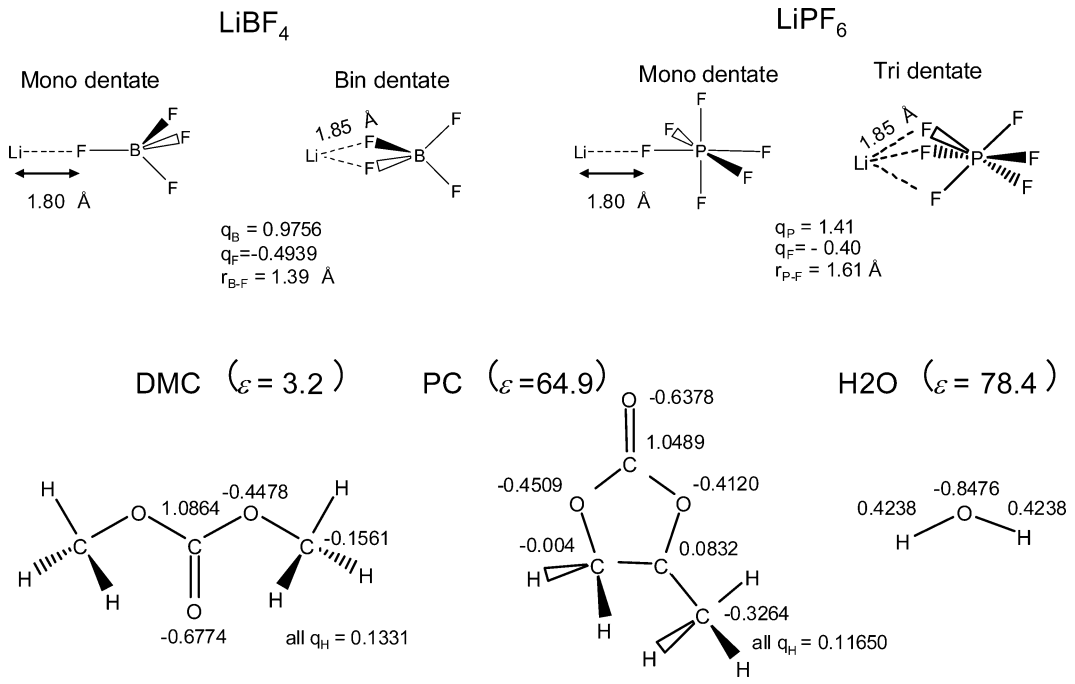

[a]The relative permittivity (ε) of solvent is shown in the parentheses.

may depend on the surrounding environment. Recently we reported conventional MD simulations for the similar concentrated solution systems (0.5 and 1.0 mol dm^{-3}) from structural and dynamical viewpoints, by which it is revealed that the monodentate ion-pair were formed as predominant species in both $LiBF_4$ and $LiPF_6$ in PC solutions.[34] On the other hand, ab initio calculations showed that the most stable structures of Li−PF_6 and Li−BF_4 ion-pairs in gas phase are tridentate[35,33] and bidentate,[36] respectively. The discrepancy between ab initio calculations and MD simulations is an indication of strong solvent effect.

In this study, we investigated the preferred structures of the CIP of Li−PF_6 and Li−BF_4 in solutions of water, PC, and DMC in terms of the solvation free energy computed by the energy representation (ER) method coupled with MD simulations. The importance of interactions of ions and/or CIP with solvent was clearly shown for the structural preference, which cannot be well captured in the continuum model describing the solvent effect by the dielectric constant.[37] The structural preference is derived not only from solute−solvent interaction but also from solvent−solvent interaction around the solute moiety. The solvent effect was also discussed in terms of empirical solvent parameters to find their connections with the present interpretation on the basis of the statistical−mechanical analyses of solvation.

2. METHOD

The contact ion-pair (CIP) formation ability in solution is described with the corresponding formation free energy in gas phase and the solvation free energies for all the species involved in the reaction. Stable structure of CIP e.g. monodentate or multidentate should depend on the solvation free energy. The CIP formation of Li^+ with BF_4^- and PF_6^- is depicted on the basis of the thermodynamic cycle represented in Chart 2. In Chart 2, ΔG^0_{gas} is CIP formation free energy in vacuum, and

Chart 2. Thermodynamic Cycle of Solvation System Including Lithium Cation Li^+, Counter Anion A^-, and Ion-Pair LiA, Where A Stands for BF_4 or PF_6

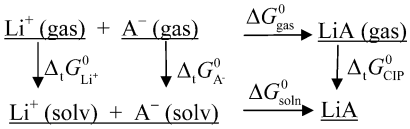

$\Delta_t G^0_{Li^+}$, $\Delta_t G^0_{A^-}$, and $\Delta_t G^0_{CIP}$ denote the solvation free energies, i.e., the transfer free energies of the lithium cation, anion, and CIP from gas phase to solutions, respectively. The standard free-energy change of CIP formation in solution ΔG^0_{soln} is then given by

$$\Delta G^0_{soln} = \Delta G^0_{gas} + \Delta_t G^0_{CIP} - (\Delta_t G^0_{Li^+} + \Delta_t G^0_{A^-}) \quad (1)$$

The relative stability of the mono- and multidentate coordination states is determined by the difference of the respective ΔG^0_{soln} through

$$\begin{aligned}\Delta\Delta G^0_{soln} &\equiv \Delta G^0_{soln}(\text{multi}) - \Delta G^0_{soln}(\text{mono}) \\ &= (\Delta G^0_{gas}(\text{multi}) - \Delta G^0_{gas}(\text{mono})) \\ &\quad + (\Delta_t G^0_{CIP}(\text{multi}) - \Delta_t G^0_{CIP}(\text{mono})) \\ &\equiv \Delta\Delta G^0_{gas} + \Delta\Delta_t G^0_{CIP}\end{aligned} \quad (2)$$

Note that the single-ion terms $\Delta_t G^0_{Li^+}$ and $\Delta_t G^0_{A^-}$ are common in the mono- and multidentate states and are canceled in eq 2. According to Chart 2 and eq 1, *the solvent effect* Δg for the CIP formation is defined as

$$\Delta g \equiv \Delta G^0_{soln} - \Delta G^0_{gas} = \Delta_t G^0_{CIP} - (\Delta_t G^0_{Li^+} + \Delta_t G^0_{A^-}) \quad (3)$$

dx.doi.org/10.1021/jp3011487 | J. Phys. Chem. B 2012, 116, 6476−6487

Table 1. Solvation Energies $\Delta_t E^0$, Solvation Free Energies $\Delta_t G^0$, Solvent Effect Δg for the Single Ions with the CIP Formation Free Energies in Vacuum ΔG^0_{gas} and in Solution ΔG^0_{soln} in kcal mol^{-1} [a]

	solvent		
	H_2O	PC	DMC
	Li^+		
$\Delta_t E^0_{Li^+}$	−219.7 ± 0.6 (−195.8 ± 0.6)	−212.6 ± 1.4 (−198.3 ± 1.4)	−220.2 ± 1.2 (−205.9 ± 1.2)
$\Delta_t G^0_{Li^+}$	−107.8 ± 0.7 (−83.9 ± 0.7)	−111.8 ± 0.8 (−97.5 ± 0.8)	−107.7 ± 0.9 (−93.4 ± 0.9)
	BF_4^-		
$\Delta_t E^0_{BF_4^-}$	−135.9 ± 0.6 (−112.0 ± 0.6)	−99.9 ± 0.9 (−85.6 ± 0.9)	−96.0 ± 1.0 (−81.7 ± 1.0)
$\Delta_t G^0_{BF_4^-}$	−81.9 ± 0.5 (−58.0 ± 0.5)	−52.1 ± 0.7 (−37.8 ± 0.7)	−53.7 ± 0.8 (−39.4 ± 0.8)

	solvent								
	H_2O			PC			DMC		
	monodentate	bindentate	difference	monodentate	bindentate	difference	monodentate	bindentate	difference
	$LiBF_4$								
ΔG^0_{gas}	−118.3	−135.3	*−17.0*	−118.3	−135.3	*−17.0*	−118.3	−135.3	*−17.0*
$\Delta_t E^0_{CIP}$	−167.7 ± 0.6	−108.8 ± 0.7	58.9	−124.9 ± 0.5	−89.0 ± 0.9	35.9	−132.3 ± 0.8	−97.5 ± 1.4	34.9
$\Delta_t G^0_{CIP}$ [b]	−79.8 ± 0.6	−49.0 ± 0.5	30.8	−57.1 ± 0.7	−40.3 ± 0.6	16.8	−60.9 ± 0.7	−44.6 ± 0.7	16.3
Δg [b]	109.9	140.7	30.8	106.9	123.7	16.8	100.4	116.7	16.3
ΔG^0_{soln}	−8.4	5.4	13.8	−11.4	−11.6	*−0.2*	−17.9	−18.6	*−0.7*

	solvent		
	H_2O	PC	DMC
	PF_6^-		
$\Delta_t E^0_{PF_6^-}$	−117.5 ± 0.5 (−93.6 ± 0.5)	−93.3 ± 1.2 (−79.0 ± 1.2)	−92.7 ± 0.9 (−78.4 ± 0.9)
$\Delta_t G^0_{PF_6^-}$	−71.2 ± 0.4 (−47.3 ± 0.4)	−48.2 ± 0.6 (−33.9 ± 0.6)	−50.8 ± 0.6 (−36.5 ± 0.6)

	solvent								
	H_2O			PC			DMC		
	monodentate	tridentate	difference	monodentate	tridentate	difference	monodentate	tridentate	difference
	$LiPF_6$								
ΔG^0_{gas}	−104.2	−120.4	*-16.2*	−104.2	−120.4	*−16.2*	−104.2	−120.4	*−16.2*
$\Delta_t E^0_{CIP}$	−170.5 ± 0.5	−116.2 ± 0.7	54.4	−139.3 ± 1.2	−93.9 ± 1.1	45.3	−141.8 ± 1.0	−103.7 ± 0.7	38.1
$\Delta_t G^0_{CIP}$ [b]	−78.0 ± 0.6	−49.0 ± 0.5	28.9	−65.1 ± 0.8	−41.3 ± 0.7	23.8	−65.3 ± 0.9	−46.6 ± 0.5	18.7
Δg [b]	101.0	129.9	28.9	95.0	118.7	23.8	93.1	111.8	18.7
ΔG^0_{soln}	−3.2	9.5	12.7	−9.2	−1.7	7.6	−11.1	−8.5	2.5

[a] The error values are shown at 95% confidence level for $\Delta_t E^0$ and $\Delta_t G^0$. The $\Delta_t E^0$ and $\Delta_t G^0$ values without the finite size correction are in parentheses (only for single ions, see eq 7). [b] As noted in the text with eq 4, the difference of ΔG^0_{CIP} between the mono- and multidentate states is the same as that for Δg.

Correspondingly, the difference $\Delta\Delta g$ of *the solvent effects* on the mono- and multidentate states is given by

$$\begin{aligned}\Delta\Delta g &\equiv \Delta g(\text{multi}) - \Delta g(\text{mono}) \\ &= \Delta_t G^0_{CIP}(\text{multi}) - \Delta_t G^0_{CIP}(\text{mono}) \\ &= \Delta\Delta_t G^0_{CIP} \end{aligned} \quad (4)$$

When calculating the solvation free energies $\Delta_t G^0_{Li^+}$, $\Delta_t G^0_{A^-}$, and $\Delta_t G^0_{CIP}$, use of such standard techniques as thermodynamic integration (TI) and free energy perturbation (FEP)[38] is restricted due to the high computational cost. Therefore, in the present work, we employ the energy representation (ER) method proposed by Matubayasi.[39−41] Compared to TI and FEP methods, the ER method can yield solvation free energy with almost the same accuracy at low computation costs,[42] and is also amenable to supercritical fluid, micelle, and lipid membrane, and quantum-mechanical/molecular-mechanical (QM/MM) system.[43−45] In the ER method of free-energy computation, the trajectories of the solution and neat solvent systems produced by MD simulations are used to determine the solvation free energy. A snapshot configuration is sampled to construct the instantaneous distribution function (histogram) of the solute−solvent intermolecular pair energy ε defined as

$$\hat{\rho}^e(\varepsilon) = \sum_i \delta(v(x_i) - \varepsilon) \quad (5)$$

where $v(x_i)$ is the pair interaction potential energy between solute molecule and solvent molecule, x_i is the configuration of the i-th solvent molecule relative to the solute molecule, and the sum is taken over all the solvent molecules. We denote the ensemble averages of $\hat{\rho}^e(\varepsilon)$ in the solution and neat solvent as $\rho(\varepsilon)$ and $\rho_0(\varepsilon)$, respectively. In the solution system, the snapshot from MD was sampled every 10 fs, and $\hat{\rho}^e(\varepsilon)$ was averaged over 2×10^4 to 4×10^4 configurations to obtain the average distribution function $\rho(\varepsilon)$. To obtain $\rho_0(\varepsilon)$, the solute was placed in the neat solvent system as a test particle; the test particle is the one placed in the solvent system without changing the solvent configuration at all. $\rho_0(\varepsilon)$ is actually equal to the density of states of the solute−solvent pair potential multiplied by bulk number density of solvent.[40] The neat solvent system was sampled every 100 fs. The test-particle

dx.doi.org/10.1021/jp3011487 | J. Phys. Chem. B 2012, 116, 6476−6487

insertion at random position and orientation was then conducted 200 times per solvent configuration sampled, leading to 2×10^5 insertions in total. Detailed description of the ER method is given in ref 40. The average sum of the solute−solvent interaction energy $\Delta_t E^0$ can also be calculated by integrating $\rho(\varepsilon)$ in the solution system;

$$\Delta_t E^0 = \int \varepsilon \rho(\varepsilon)\, d\varepsilon \tag{6}$$

Although this is not experimentally measurable, it is the major part of the enthalpy of solvation when the solute is an ion or a CIP.

In MD simulations, the CIP coordination structures are fixed, in which BF_4^- and PF_6^- were kept tetrahedral and octahedral symmetry, respectively. CIP geometries are shown in Chart 1. Also structures of the solvents examined are shown in Chart 1. The monodentate Li−BF_4 and Li−PF_6 were generated by setting the Li cation to the collinear positions of the adjacent F atom and the B and P atoms, respectively. In the case of Li−BF_4 bidentate, Li atom is at the same distances from the two, adjacent F atoms and is placed on the plane defined by the two F atoms and the B atom. The Li−PF_6 tridentate form was made by placing a Li atom at the same distances from the three, adjacent F atoms; Li and three F form a triangular pyramid. The distance between the Li atom and the adjacent F atom was then varied within the above structural constraints to minimize the ion−ion potential energy within the classical force field described below. The distance corresponding to the minimum energy determines the target ion-pair configuration of the present work, and is shown in Chart 1. The ion−ion potential energy at that configuration is the free energy of CIP formation in vacuum ΔE^0_{gas} in Table 1. The SHAKE algorithm[46] was used to constrain the bonds in PC and DMC molecules and the rigid model was adopted for $LiBF_4$, $LiPF_6$, and H_2O molecules.

Water is the most common solvent for ions so that thermodynamic quantities have been accumulated so far. PC and DMC are cyclic and acyclic molecules, respectively, thus the topological difference is evident between them. The SPC/E model[47] was used for water. The CIPs, the single anions, and water were treated as rigid, while only the bond-lengths were fixed for PC and DMC. The other intramolecular flexibilities of PC and DMC were explicitly taken into account. The force fields used in our previous study[34] were employed for the single ions, CIPs, PC, and DMC. The geometric mean was adopted for combining both the Lennard-Jones parameters σ and ε of unlike atoms, thus, $\sigma_{ij} = (\sigma_{ii}\sigma_{jj})^{1/2}$, $\varepsilon_{ij} = (\varepsilon_{ii}\varepsilon_{jj})^{1/2}$. The Lennard-Jones and Coulomb potentials were incorporated into the intramolecular interactions of PC and DMC only for the pairs of atoms with three-bond separations (1−4 interaction) or with more separations. The intramolacular 1−4 interaction was scaled by factors of 0.50 and 0.833 for the Lennard-Jones and Coulomb parts, respectively.

For the ER method, the solution system contained a single solute species (ion or ion-pair) and 256 solvent molecules, and solvent molecules of the same number were used in the neat solvent system. The equation of motion was solved with the Gear predictor-corrector method[38,48] at a time step of 0.5 fs in the canonical ensemble; the temperature was set at 298 K and the unit cell was taken to be cubic. The box size L is common between the corresponding solution and neat solvent systems, and was set to 19.71, 33.01, and 32.95 Å for water, PC, and DMC, respectively by referring the experimental densities.[49] The periodic boundary condition was employed in the minimum image convention, and the electrostatic potential was handled by the Ewald method. The screening parameter was set to $2.8/L$, and the reciprocal vectors with $n_x^2 + n_y^2 + n_z^2 \leq 27$ were used. The truncation at 10 Å was applied on the site−site basis to the real-space part of the electrostatic interaction in the Ewald method and the Lennard-Jones part of the intermolecular interaction. When the solute has a net charge, the finite-size correction term was added to the solvation free energy $\Delta_t G^0$ and the average sum of the solute−solvent interaction energy $\Delta_t E^0$. According to the standard procedure,[50] the correction $\Delta\xi$ is expressed as

$$\Delta\xi = -\frac{2.8}{2L} q^2 \ (\text{kcal mol}^{-1}) \tag{7}$$

where q is the total charge of the solute.

The simulation length for equilibration was 100 ps for all the systems. The production run was performed over a duration which gives the error at 95% confidence level of 1 kcal mol^{-1} for $\Delta_t E^0$ and $\Delta_t G^0$, i.e. over 200 ps for the solutions of Li−PF_6 tridentate and Li−BF_4 bidentate ion-pairs, over 400 ps for Li−PF_6 monodentate and Li−BF_4 monodentate ion-pairs, over 300 ps for Li^+, BF_4^-, and PF_6^- single ions, and over 100 ps for all the neat solvents. All the MD simulations were performed using Materials Explorer 4.0 and Materials Explorer 4.0/MD software packages (FUJITSU Ltd.).[51]

3. RESULTS AND DISCUSSION

Our target is the contact ion-pairs (CIP), and we show and discuss the results in three subsections. In subsection 3.1, we describe the solvation of single ions of Li^+, BF_4^-, and PF_6^-. In subsection 3.2, we examine the solvation of CIPs of $LiBF_4$ and $LiPF_6$ in strong connections to the coordination structures. In subsection 3.3, we discuss the CIP formation on the basis of the results in subsections 3.1 and 3.2. All the relevant values of the calculated solvation free energy $\Delta_t G^0$ and the solute−solvent interaction energy $\Delta_t E^0$ are summarized in Table 1.

3.1. Single-Ion Solvation. Among the investigated systems, the hydration of Li^+ is the most suitable to validate the force fields and methodology employed here, because several experimental[52−54] and theoretical[31,32,55−57] studies have been reported. Our value of $\Delta_t G^0_{Li^+} = -107.8$ kcal mol^{-1} is in agreement with the experimental values of $\Delta_t G^0_{Li^+}$ is −113.5[52] or −113.8[53] kcal mol^{-1} within 5% accuracy. Joung have reported the value of −113.3 kcal mol^{-1} based on the newly developed force fields,[56] and also assessed previous force fields developed by Jensen et al.[55] and Aqvist.[31] These force fields yield the hydration free energies of −105.6 and −108.1 kcal mol^{-1}, respectively. Employed Lennard-Jones parameters for Li in this study have been originally constructed for nonaqueous solvents by Soetens and co-workers.[29] In PC, the present $\Delta_t G^0_{Li^+}$ value of −111.8 kcal mol^{-1} is also in agreement with the experimental value of −107.8 kcal mol^{-1}[58] within 5% accuracy. A significant deviation between experimental (−45 kcal mol^{-1}[52]) and calculated (−81.9 kcal mol^{-1}) has been found in $\Delta_t G^0$ for BF_4^- in water, possibly due to the insufficient treatment of the charge distribution of BF_4^-. It was seen with QM/MM simulation[59,60] that the reduction of electron density into a set of point charges has a significant effect on the energetics of anion, though the effect will be less serious on the energetics of the CIP formation due to the cancellation of errors. For the other cases, neither experimental nor computational values have been reported for single-ion solvation.

dx.doi.org/10.1021/jp3011487 | J. Phys. Chem. B 2012, 116, 6476−6487

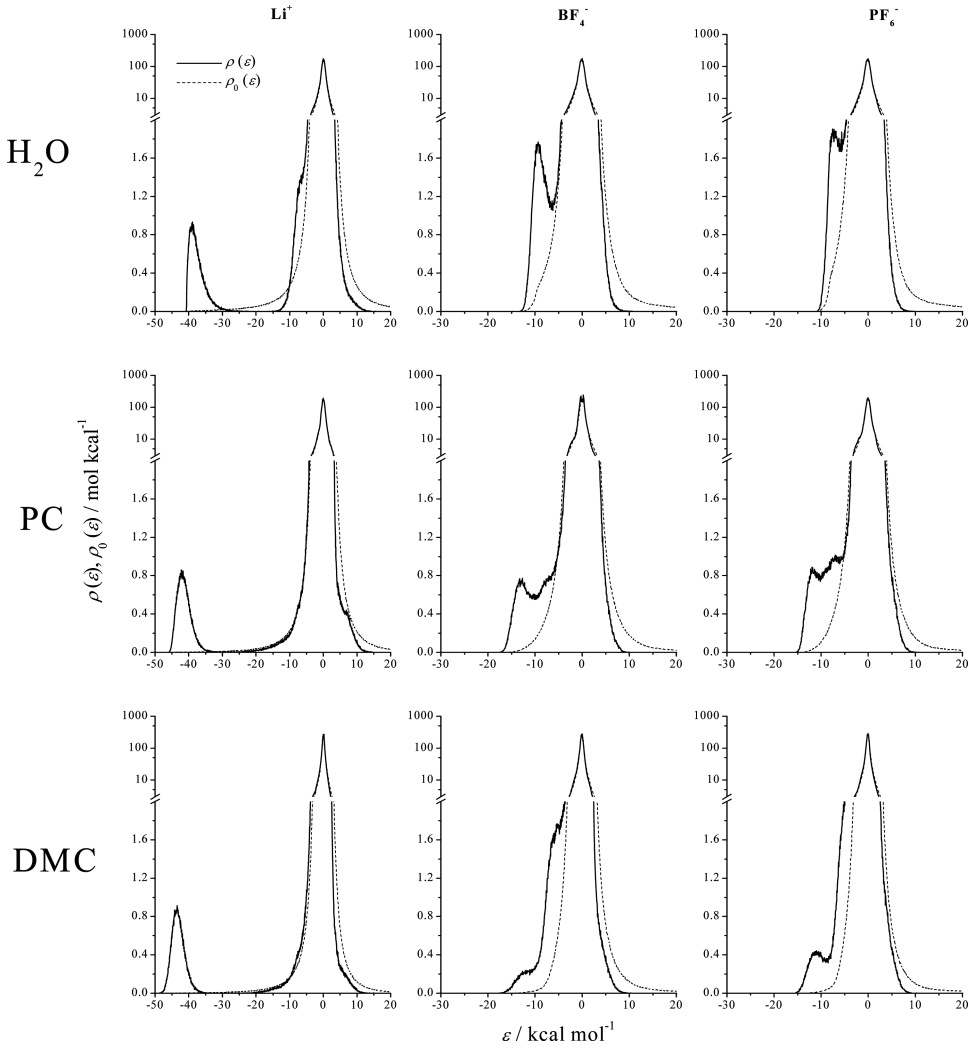

Figure 1. Distribution functions $\rho(\varepsilon)$ and $\rho_0(\varepsilon)$ of the pair interaction energy ε of single ion with solvent. Note a break of ordinate at 2 mol/kcal. The ordinate is linearly graduated below this value, and is logarithmically graduated above it.

The order of $\Delta_t G^0$ was $Li^+ < BF_4^- < PF_6^-$ in all solvents. According to the Hofmeister series,[61] hydration is stronger for BF_4^- than for PF_6^- because of higher surface charge density of BF_4^- relative to PF_6^- (see CHART 1). Interestingly, the same order as the Hofmeister series for hydration has been observed for solvation in carbonate solvents. Comparing solvent species, $\Delta_t G^0$ s of Li^+ are almost the same in all solvents, though $\Delta_t G^0_{Li^+}$ in PC is slightly smaller than in DMC and water. For the anions, the order of $\Delta_t G^0_{X^-}$ values is (in water) ≪ (in DMC) < (in PC), which is easily expected from greater electron pair accepting nature of water. The $\Delta_t G^0_{X^-}$ in DMC is slightly lower than in PC both for BF_4^- and PF_6^-.

The distribution functions of the solute−solvent pair energy $\rho(\varepsilon)$ for single ions are shown in Figure 1. The negative and positive regions of ε refer to the attractive and repulsive interactions between solute and solvent, respectively. The intense peak around 0 appears in all the $\rho(\varepsilon)$ due to the far-separated solute−solvent pairs. Other peaks in negative side express the attractive solute−solvent pair energies, e.g., the peak at −38 kcal mol^{-1} in $\rho(\varepsilon)$ of Li^+ in water originates from the most attractive water molecules in the first nearest neighbors of the Li^+, and the shoulder at negative envelope near the intense peak arises from the waters in the outer solvation shells. The solute−solvent interaction energy $\Delta_t E^0$ is calculated from $\rho(\varepsilon)$ as shown in eq 6. Note that the $\Delta_t E^0$ value without the finite size correction (values in parentheses in Table 1) corresponds to the $\rho(\varepsilon)$ profile. The order of $\Delta_t E^0$ for ionic species in all the solvents is consistent with that of attractive peak positions in negative region of $\rho(\varepsilon)$, i.e., $Li^+ < BF_4^- < PF_6^-$ for all the solvents (see Table 1 and Figure 1), and the order is same as the order of $\Delta_t G^0$. Also the order of $\Delta_t E^0_{Li^+}$ for different solvents is consistent with the peak position in $\rho(\varepsilon)$, i.e., DMC < PC < H_2O.

$\rho(\varepsilon)$ describes the energetic correlation, while radial distribution function $g(r)$ and running integrals $n(r)$ represent the spatial correlation features. Figure 2 shows $g(r)$s and $n(r)$s in H_2O derived from MD trajectory data. $g_{Li-O}(r)$ and $n_{Li-O}(r)$ illustrate that the Li^+ hydration structural features such as bond length and coordination number agree with those previously published.[34] The broad peak at ca. 4 Å, which is about twice of 2 Å, indicates the second hydration shell. In the corresponding $\rho(\varepsilon)$, the shoulder at −9 kcal mol^{-1} is about quarter in energy of the lower peak at −38 kcal mol^{-1}, which corresponds to the fact that the charge-dipole interaction is in inverse proportion to the distance squared. The order of the strength of the first-peak coordination represented by $dg_{Li-O}(r)$ with d the number of bulk solvent is H_2O < PC < DMC, which is consistent with the order of $\Delta_t E^0_{Li+}$ in parentheses in Table 1.

dx.doi.org/10.1021/jp3011487 | J. Phys. Chem. B 2012, 116, 6476−6487

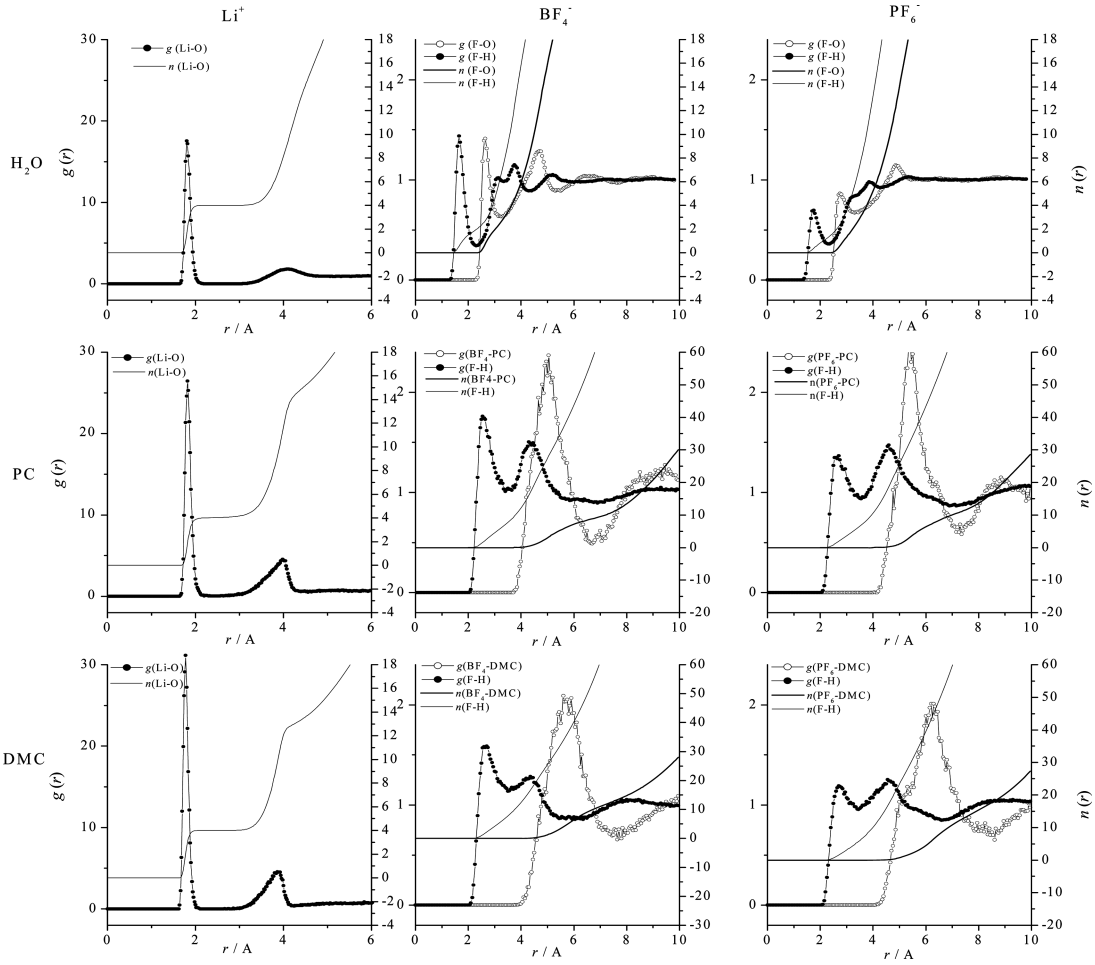

Figure 2. The radial distribution functions $g(r)$ and running integrals $n(r)$ of single-ions. The expressions of BF_4-PC, BF_4-DMC, PF_6-PC, and PF_6-DMC refer to the distances between the centers of mass.

As for anions, both the first-peaks in $g_{F-H}(r)$ and in $g_{F-O}(r)$ for BF_4^-/H_2O are stronger than the corresponding peaks for PF_6^-/H_2O. The second peak in $g_{F-O}(r)$ is clearly seen only for BF_4^-/H_2O. Also $n_{F-H}(r)$s reveal that about two H atoms of water molecules bind to each F atom of BF_4^- in average, while less than two H atoms bind to F atom of PF_6^-, which proves that water molecules more tightly bind to BF_4^- than to PF_6^-. Comparison of $g_{F-H}(r)$ of BF_4^-/PC and BF_4^-/DMC shows that the two peaks at 2−5 Å are larger and sharper for BF_4^-/PC than the corresponding peaks of BF_4^-/DMC. It means that PC coordinates more tightly to BF_4^- than DMC. This is supported by $\rho(\varepsilon)$. In terms of $\rho(\varepsilon)$, the first peak in BF_4^-/PC at −13 kcal mol^{-1} has higher intensity than the corresponding peak in BF_4^-/DMC, which means that PC coordinates more rigidly with BF_4^- than DMC in the first solvation shell. Meanwhile, the shoulder at −6 kcal mol^{-1} is clearly visible in BF_4^-/DMC, which suggests that the favorable interactions in outer region is more abundant for DMC. Since the contribution from the shoulder is added in eq 6 to the primary peak at −13 kcal mol^{-1}, $\Delta_t E^0_{BF_4^-}$ in PC is only 4 kcal mol^{-1} lower than $\Delta_t E^0_{BF_4^-}$ in DMC. A similar remark applies to PF_6^-, and $\Delta_t E^0_{PF_6^-}$ in PC is almost the same as in DMC.

For repulsive interaction between anion and carbonate solvent, the envelope on positive side in $\rho(\varepsilon)$of anion−DMC is narrower than that in $\rho(\varepsilon)$ of anion−PC, especially for BF_4^-, which is due to the conformational changes and coordination flexibility of DMC[10] unlike cyclic molecule PC. PC interacts via methyl and methylene groups with F of anion stably, to form a shoulder in the negative ε region. At the same time, electrostatic repulsion between electronegative three O of PC and F of anions delivers the wider envelope in the positive ε region than the DMC case. This interpretation is supported by structural view, in which all the peaks in the $g(r)$ of anions with PC are located at shorter distance and sharper than the corresponding peaks with DMC, which confirms that PC binds rigidly and repulsively to anions while DMC binds more flexibly.

The difference between $\Delta_t G^0$ and $\Delta_t E^0$ is derived from the profile difference between $\rho(\varepsilon)$ and $\rho_0(\varepsilon)$ as described in the previous paper.[44] $\rho(\varepsilon)$ is the distribution of the pair energy ε in the solution system of interest, while $\rho_0(\varepsilon)$ is the density of states of the solute−solvent potential function multiplied by the bulk solvent density. In obtaining $\rho_0(\varepsilon)$, the statistical ensemble is generated through a test-particle procedure described in Sec II without physically coupling solute and solvent. The variation from $\rho(\varepsilon)$ to $\rho_0(\varepsilon)$ is caused by the introduction of solute−solvent interaction, and reflects the effect of solvent reorganization. When $\rho(\varepsilon)$ and $\rho_0(\varepsilon)$ are more different, $(\Delta_t E^0 - \Delta_t G^0)$ is more positive.

In Li^+ solvation, $(\Delta_t E^0 - \Delta_t G^0)$ values are more than 100 kcal mol^{-1} for any solvent. As shown in Figure 1 the profile difference is mainly in negative side, thus Li^+−solvent attractive peak appears at ca. −40 kcal mol^{-1} only in $\rho(\varepsilon)$. Since the peak

dx.doi.org/10.1021/jp3011487 | J. Phys. Chem. B 2012, 116, 6476−6487

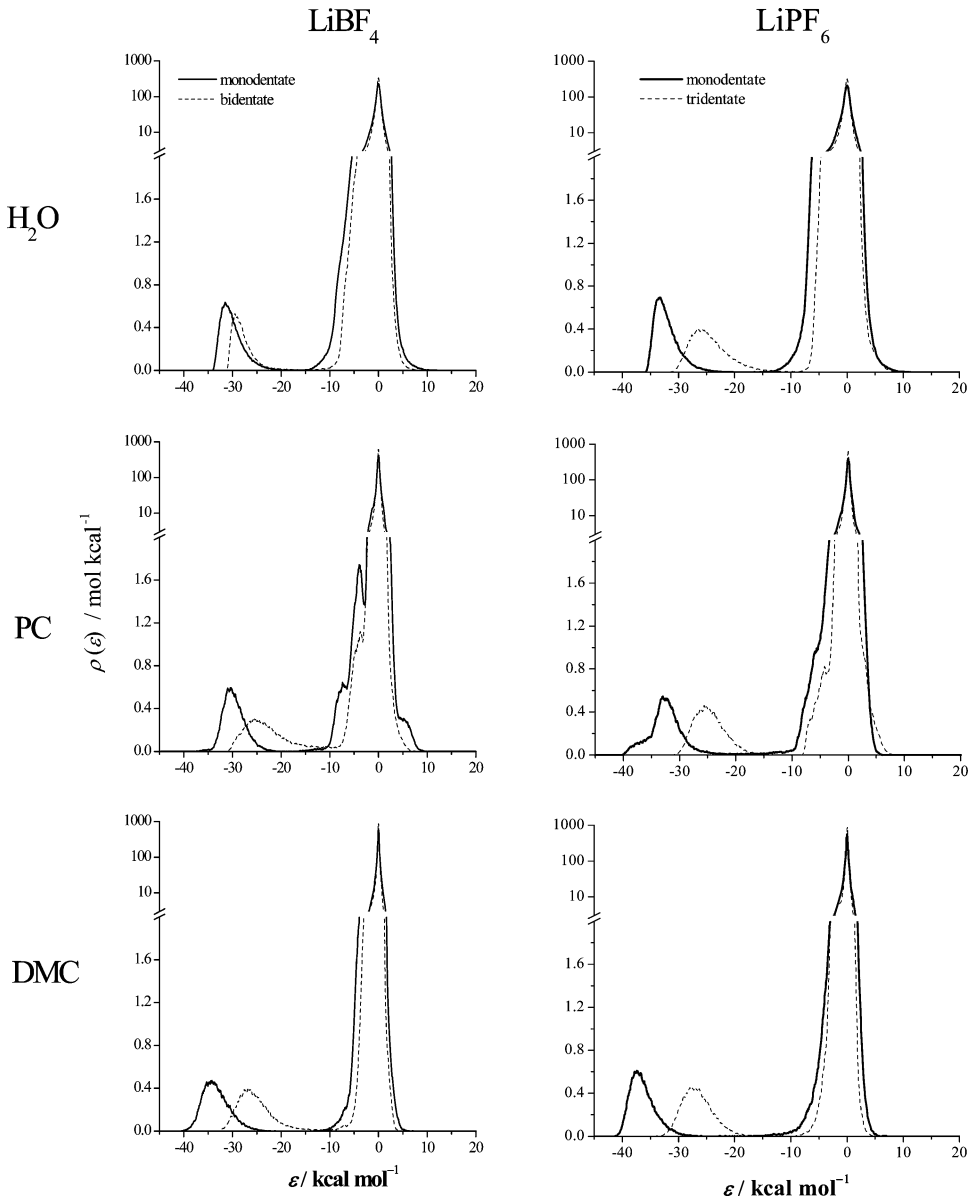

Figure 3. Distribution function $\rho(\varepsilon)$ of the pair interaction energy ε of CIP with solvent. Note a break of ordinate at 2 mol/kcal. The ordinate is linearly graduated below this value, and is logarithmically graduated above it.

position of Li^+ is lower than those of anions for any solvent, the $(\Delta_t E^0 - \Delta_t G^0)$ values for Li^+ are larger than the corresponding values for anions. The lithium cation makes a rigid hydration shell because of its small size and strong electric field.[62,63] It brings the first sharp peak in $g(r)$ as structural feature, the attractive peak of $\rho(\varepsilon)$ in the low-energy region as energetic feature, and the large $(\Delta_t E^0 - \Delta_t G^0)$ value as thermodynamic property. Moreover, the detailed comparison of the Li^+ solvation in PC and DMC reveals that the attractive Coulomb interaction between Li^+ and O atoms of DMC is stronger than in PC since atomic charge of carbonyl oxygen of DMC is more negative than of PC as shown in Chart 1. This is the main reason why $\Delta_t E^0_{Li+}$ in DMC is more negative than that in PC. However, the solvation free energy $\Delta_t G^0_{Li+}$ is more negative in PC than in DMC, and the order is reversed from that of $\Delta_t E^0_{Li+}$. Since the profile difference in Li^+/DMC is larger than in Li^+/PC, the $(\Delta_t E^0_{Li^+} - \Delta_t G^0_{Li^+})$ in DMC is larger than in PC. From structural point of view, the first-peak in $g_{Li-O}(r)$ of Li^+/DMC is higher in intensity than in Li^+/PC regardless of same coordination number of O atom. Thus, the peak in PC is broader than in DMC, suggesting that the solvation of Li^+ in PC is entropically more favorable than in DMC and that $\Delta_t G^0_{Li^+}$ in PC is lower than in DMC. Additionally, DMC is a flexible molecule with two stable conformations, e.g., trans−trans as shown in Chart 1 and trans−cis. Favorable solvation of trans−cis isomer to Li^+ has been suggested by Raman spectroscopy relative to the other.[64] As DMC itself has conformational flexibility, four DMC molecules can adjust their conformational structures to coordinate Li^+. The tightly coordinated structure provides entropic disadvantage to the solvation of Li^+ in DMC.

As mentioned above, all the $g(r)$ peaks of the anions in PC are higher than in DMC. Since the number densities in the bulk are almost the same between PC and DMC, this is consistent with the result that both $\Delta_t E^0_{BF_4^-}$ and $\Delta_t E^0_{PF_6^-}$ in PC are smaller than in DMC. On the other hand, both $\Delta_t G^0_{BF_4^-}$ and $\Delta_t G^0_{PF_6^-}$ in PC are larger in DMC. Figure 1 shows that the "difference" between $\rho(\varepsilon)$ and $\rho_0(\varepsilon)$ is larger in PC than in DMC, which is

dx.doi.org/10.1021/jp3011487 | J. Phys. Chem. B 2012, 116, 6476−6487

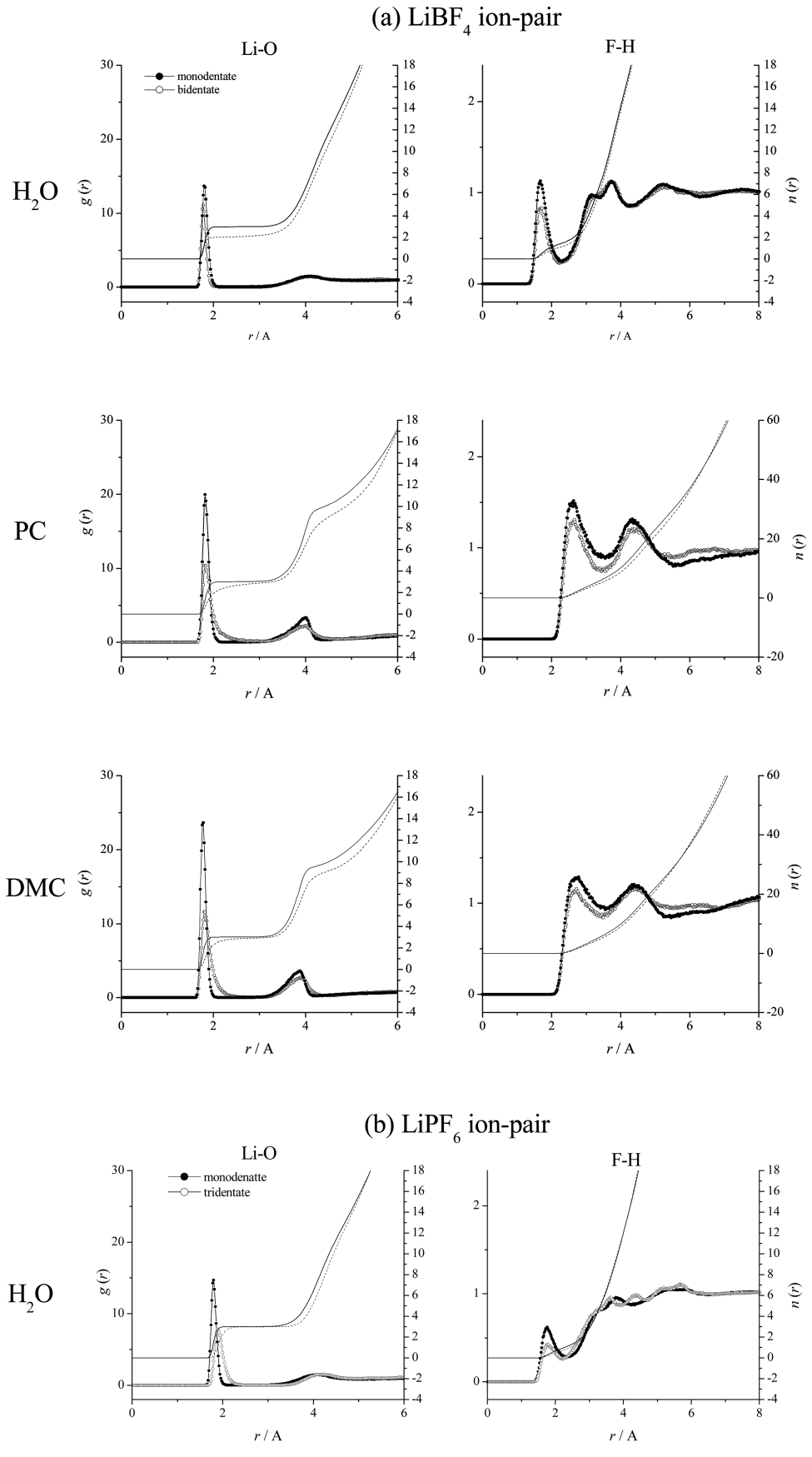

Figure 4. continued

dx.doi.org/10.1021/jp3011487 | J. Phys. Chem. B 2012, 116, 6476−6487

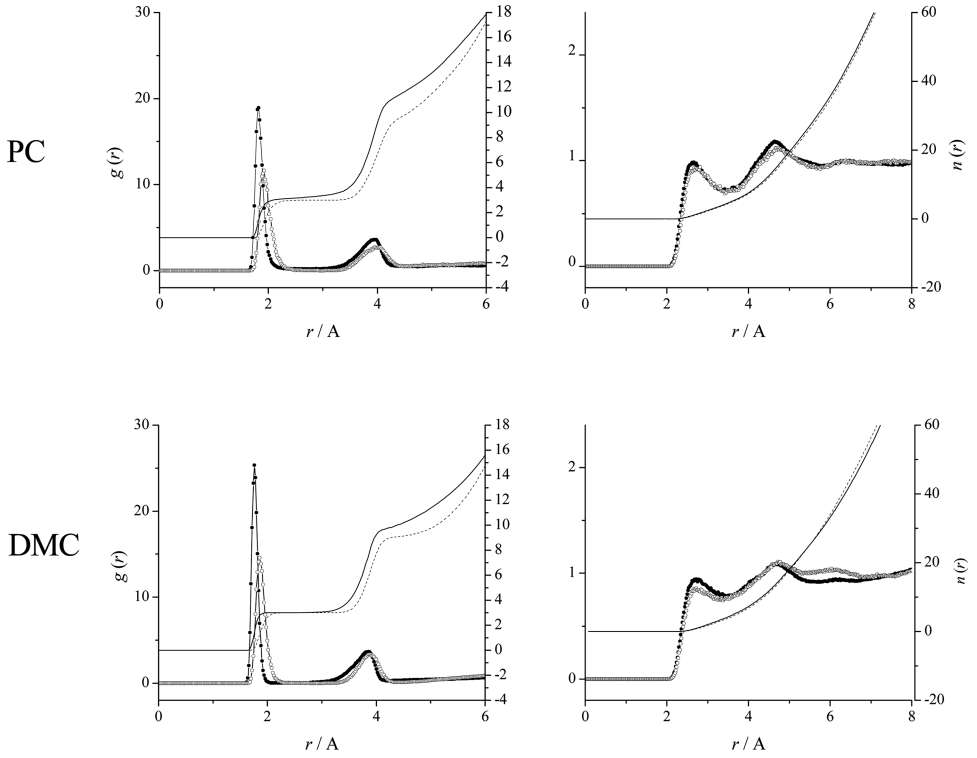

Figure 4. Radial distribution functions $g(r)$ of monodentate (full circle) and multidentate (open circle) states accompanied by the corresponding running integrals $n(r)$ of monodentate (full line) and multidentate (dash line) states.

in correspondence to the observation in Figure 2 that $g(r)$ is sharper in PC. This reads to the larger solvent reorganization in PC, and $(\Delta_t E^0_{X^-} - \Delta_t G^0_{X^-})$ is larger in PC than in DMC for the anionic solutes BF_4^- and PF_6^-. It is of interest to note that the role of solvent reorganization in PC and DMC is reserved between Li^+ and anions.

It is a common practice to describe the solvation phenomena in terms of empirical solvent parameters, and we will discuss their connections to the present results. The relative permittivity (ε) of DMC is much smaller than those of water and PC; i.e., ε (at 298 K) = 78.4, 64.9, 3.2 for water, PC and DMC, respectively. One may expect that the ionic solvation is much less favorable in DMC than in the others. In fact, according to the Born model with ionic radii for the 4-coordinated lithium ion of 0.59 Å,[65] solvation free energies of Li^+ are estimated to be −277.8, −277.0, and −190.5 kcal mol^{-1} in water, PC and DMC, respectively.[49] Of course, though rough, such continuum models based on the relative permittivity fail to describe the Li^+ solvation since Table 1 shows that the free energy of Li^+ solvation $\Delta_t G^0_{Li^+}$ depends weakly on the solvent species. On the other hand, the computed $\Delta_t E^0_{Li^+}$ are in the same order as the Gutman's donor numbers (DN); 15.1 and 17.2 kcal mol^{-1} for PC and DMC, respectively. DN is a measure of the electron-pair donating ability of the solvent and is defined as a reaction enthalpy for the reaction $SbCl_5 + Cl^- \rightarrow SbCl_6^-$ in solution system.

More negative values of anion's $\Delta_t E^0_{X^-}$ in water than in carbonate solvents can be explained by solvent property as the electron pair acceptor. The Gutmann and Mayer's acceptor number (AN)[66] and Reichardt's betaine E_T (30)-parameter[67] are good measures to evaluate the electron pair accepting ability. The AN values are 54.8 and 18.3[49] for water and PC, respectively and E_T (30) values are 63.1, 46.0 and 38.2[49] for water, PC and DMC. The order of $\Delta_t E^0_{X^-}$ agrees with the order of AN and E_T (30) completely. Additionally as mentioned before, the order of $\Delta_t E^0$ is coincident with the order of the peak position in $\rho(\varepsilon)$ for Li^+, BF_4^- and PF_6^-. Thus, our energetic analysis based on all-atom simulation and statistical-mechanical treatment of solution is in good correspondence with the conventional, empirical-parameter analysis, and furthermore, provides the free-energy values quantitatively.

3.2. CIP Solvation for Different Coordination Forms.

With regard to the monodentate CIPs, it is worth mentioning that $\Delta_t E^0_{CIP}$ value for $Li-PF_6$ is more negative than for $Li-BF_4$ in all of the solvents, though the reverse is the case in $\Delta_t E^0_{X^-}$ for single anions. In $\rho(\varepsilon)$ (Figure 1 and 3), the peak position in the attractive interaction side ranging from −45 to −30 kcal mol^{-1} is on the order of Li^+ < $Li-PF_6$ < $Li-BF_4$ in all of the solvents. On the other hand, the interaction at the moiety of anion appears just as the shoulder at around −10 kcal mol^{-1}, and there is no significant difference between $Li-BF_4$ and $Li-PF_6$. These suggest that the order of $\Delta_t E^0$ is dictated by the interaction around the Li^+ moiety of CIP rather than the anion part, as expected because $\Delta_t E^0$ of single ion Li^+ is much larger in magnitude than that of single anions BF_4 and PF_6. Although steric hindrance between the anion moiety and solvents molecules around the Li^+ part in the CIPs would be larger for $Li-PF_6$, $\Delta_t E^0_{CIP}$ for $Li-PF_6$ is noticeably more negative than for $Li-BF_4$, suggesting that the electrostatic repulsion among three atoms of solvent oxygen and CIP fluorine plays an important role because charge of fluorine of $Li-BF_4$ is more negative than that of $Li-PF_6$ in CHART 1. Figure 4 shows $g(r)$ and $n(r)$ of Li − O and F − H for water, PC, and DMC. From the structural viewpoint, the Li^+-O bond length is practically identical for both monodentate CIPs. $\Delta_t G^0_{CIP}$ difference between $Li-BF_4$ and $Li-PF_6$ is smaller than that in $\Delta_t E^0_{CIP}$, implying that the excluded-volume effect for $Li-PF_6$ is larger

dx.doi.org/10.1021/jp3011487 | J. Phys. Chem. B 2012, 116, 6476−6487

than for Li−BF_4. since the anion part in Li−PF_6 is more bulky as shown in CHART 1.

$\Delta_tG^0_{CIP}$ and $\Delta_tE^0_{CIP}$ for the monodentate states of Li−BF_4 and Li−PF_6 are much more negative than the corresponding values for the multidentate (bidentate and tridentate) states regardless of the solvent species. The difference in $\Delta_tG^0_{CIP}$ between the monodentate and multidentate states is smaller than that in $\Delta_tE^0_{CIP}$ in all of the cases. When $\Delta_tE^0_{CIP}$ is larger in magnitude, the solvent reorganization from neat phase to solvation phase is also larger. The compensation of $\Delta_tE^0_{CIP}$ and the solvent reorganization is then more strongly operative for the monodentate state than for the multidentate state, and reduces the difference of $\Delta_tG^0_{CIP}$ between the mono- and multidentate state.

The $n_{Li-O}(r)$ in Figure 4 shows that three solvent molecules exist in the first solvation shells around the Li^+ cation moiety for all of the CIPs except for the bidentate Li−BF_4 in water. The numbers of coordination from the anion and solvent molecules are summed into 4. For bidentate Li−BF_4 in water, $n_{Li-O}(r)$ shows the presence of only two water molecules around the Li^+ moiety, which lead to 58.9 kcal mol^{-1} more positive $\Delta_tE^0_{CIP}$ for the bidentate Li−BF_4 than for the monodentate one. In the carbonate solutions, the difference in $\Delta_tE^0_{CIP}$ between the mono- and tridentate state for Li−PF_6 is larger than that between the mono- and bidentate state for Li−BF_4, which will be discussed in detail on the structural viewpoint.

The first-peaks at around 1.8 Å in monodentate $g_{Li-O}(r)$ are slightly higher and narrower than the corresponding peaks in multidentate $g_{Li-O}(r)$. Moreover the first peak for the multidentate CIPs noticeably stretches toward large distances except for the bidentate Li−BF_4 in water, suggesting that the Li^+ moiety in the monodentate CIPs is more tightly bound to solvent molecules than the multidentate ones, since at the multidentate state, a high packing is enforced among solvating solvents and the repulsive effect is operative. For the Li−BF_4 CIPs, the positions of the first peaks in $g_{Li-O}(r)$ for all of the solvents are almost the same between the mono- and bidentate CIPs. For the Li−PF_6, on the other hand, the Li−O distances in the tridentate CIPs are slightly longer than the monodentate one because of larger electrostatic repulsion in the tridentate. The differences lead to the observation in PC and DMC that the difference in $\Delta_tE^0_{CIP}$ between the mono- and multidentate states is larger for Li−PF_6 than for Li−BF_4.

For the anionic part of CIPs, the first peak positions in $g_{F-H}(r)$ and coordination numbers are almost the same in Li−BF_4 and Li−PF_6, and the first-shell solvents are located more distantly by ca. 0.7 Å in PC and DMC than in water. This indicates that water molecules locate more closely to the anionic part of CIP owing to much greater hydrogen bonding ability. In addition steric and electrostatic repulsions among solvating carbonate molecules operate. This is consistent with $\Delta_tE^0_{CIP}$, that is, water is energetically more favorable than the carbonate solvents for both Li−BF_4 and Li−PF_6. The oscillation amplitudes in $g_{F-H}(r)$ for the monodentate CIPs in both carbonate solvents are larger than for the multidentate ones except for Li−PF_6 in PC. In particular, the second minimum is clearly seen around 5.5 Å in $g_{F-H}(r)$ for the monodentate CIPs, showing the formation of well-defined solvation layers. These features in $g_{F-H}(r)$ indicate that solvents around anionic part moiety of the monodentate CIPs are more ordered, and that the freedom of motions for such solvents is restricted to reduce entropy comparing to the multidentate states.

$\rho(\varepsilon)$ of CIP in Figure 3 reflects solute−solvent energetics depending on the coordination structure. A distinct peak is present at −43 to −38 kcal mol^{-1} in the single-ion Li^+ $\rho(\varepsilon)$ (Figure 1), and the corresponding peak in the CIP $\rho(\varepsilon)$ from solvents around the Li^+ moiety shifts at −40 to −25 kcal mol^{-1}. The order of the peak positions is (single-ion Li^+) < (monodentate CIP) < (multidentate CIP), and the peak position strongly correlates with $\Delta_tE^0_{CIP}$ of eq 6 as well as the solvation free energy $\Delta_tG^0_{CIP}$ for all of the CIPs. Although the peak positions of $\rho(\varepsilon)$ are close between the mono- and bidentate Li−BF_4 CIPs in water, the former has a larger hydration number as mentioned with respect to Figure 4(a). $\Delta_tG_{CIP}{}^0$ and $\Delta_tE_{CIP}{}^0$ in the carbonate solvents are less negative than in water for all the CIPs. This tendency is similar to $\Delta_tG^0_X$ and $\Delta_tE^0_X$ for a single anion. Such a negative $\Delta_tE^0_{CIP}$ in water arises from the strongest hydrogen bonding accepting ability of water.

The spatial distribution functions (SDF) of oxygen atom in water and of carboxyl oxygen in PC and DMC are shown in Figure 5. Highly symmetrical (ring like) distributions are found around the Li^+ moiety of the monodentate CIP for both Li−BF_4 and Li−PF_6 (Figure 5, parts a, c, e, g, i, k). For the multidentate CIP, on the other hand, favorable coordination by the solvent is scattered and spatially more restricted (Figure 5, parts b, d, f, h, l). This leads to the weaker solvation for the multidentate state seen as the smaller and broader in the first peak of $g_{Li-O}(r)$ (Figure 4) and the less negative and less distinct in negative-ε peak of $\rho(\varepsilon)$ (Figure 3). As for the bidentate Li−BF_4 CIP in water (Figure 5b), two isolated distributions are present in upper and lower sides of Li−F−F−B plane and a tetrahedral-like structure is made by two fluorine atoms of BF_4 anions and two oxygen atoms of water molecules. The tetrahedral structure forms to reduce the electrostatic repulsion between two fluorine atoms and two oxygen atoms since the water oxygen has a relatively high, partial charge.

3.3. CIP Formation Free Energy. To discuss CIP formation ability in solution, $\Delta_tG^0_{soln}$ was calculated with eq 1 and shown in Table 1. The differences between the mono- and multidentate CIPs $\Delta\Delta G^0_{soln}$ of eq 2 are also shown with the CIP formation energy differences in vacuum $\Delta\Delta G^0_{gas}$ and the *solvent effect* differences $\Delta\Delta g$ of eq 4. In vacuum, $\Delta\Delta G^0_{gas}$ of the bidentate Li−BF_4 is 17.0 kcal mol^{-1} more stable than of the monodentate. In the aqueous solution, on the other hand, the solvent effect on the bidentate is 30.8 kcal mol^{-1} larger than of the monodentate. Thus, the monodentate Li−BF_4 formation free energy ΔG^0_{soln} becomes more favorable by 13.8 kcal mol^{-1} in water than the bidentate one. Similarly, the solvent effect dominates over the gas-phase energy for the mono- and tridentate states of Li−PF_6. Namely the monodentate Li−PF_6 is more favorable by 12.7 kcal mol^{-1} than tridentate. Thus, both of the monodentate Li−BF_4 and Li−PF_6 CIPs are formed in water favorably over the corresponding multidentate ones.

When the ion-pair is Li−BF_4 and the solvent is PC or DMC, $\Delta\Delta g$ between mono- and bidentate is close to the corresponding $\Delta\Delta G^0_{gas}$ in magnitude. $\Delta\Delta G^0_{soln}$ is then close to zero, and the amounts of monodentate and bidentate CIPs are expected to be comparable to each other. When the ion-pair is Li−PF_6, $\Delta\Delta g$ between mono- and tridentate surpasses $\Delta\Delta G^0_{gas}$ in both of PC and DMC. The Li−PF_6 results are consistent with our previous result[34] and are in agreement with Borodine's for $LiPF_6$ in DMC and EC: DMC mixed solvents.[33] The order

dx.doi.org/10.1021/jp3011487 | J. Phys. Chem. B 2012, 116, 6476−6487

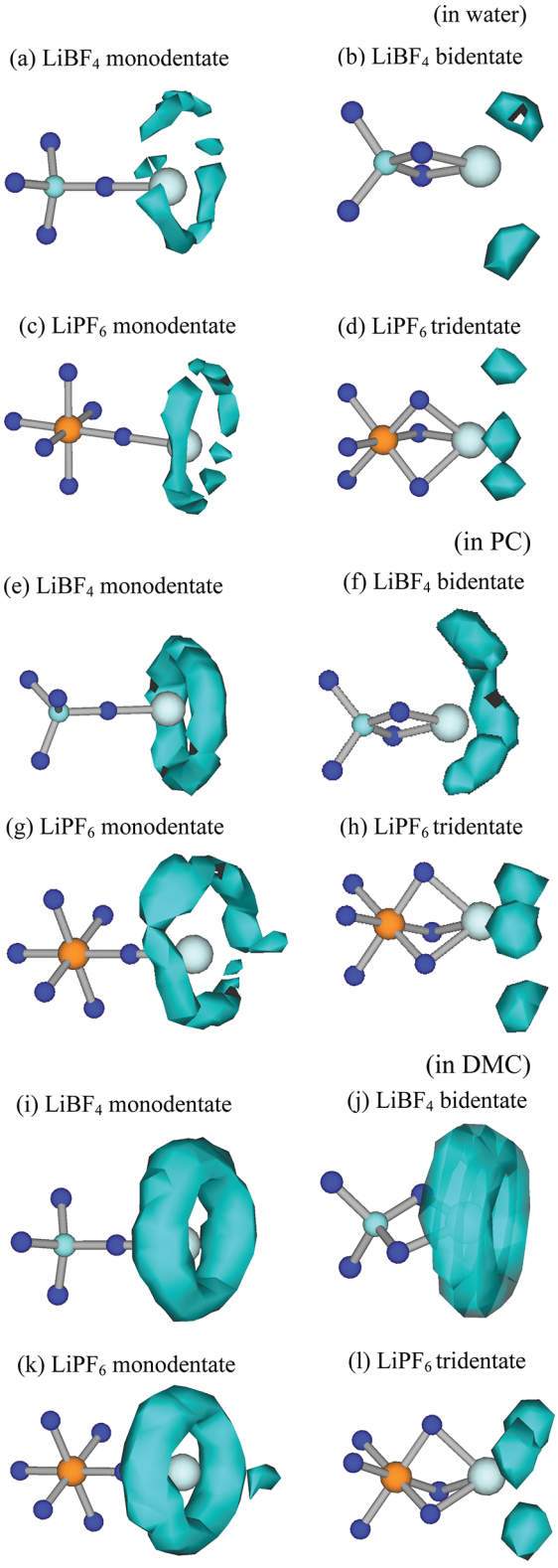

Figure 5. Spatial distribution function (SDF) of the solvent oxygen atom (carbonyl oxygen atom in the cases of PC and DMC) around an ion pair (a–d) in water, (e–h) in PC, and (i–l) in DMC at the oxygen density of 10 times the bulk value.

of ΔG^0_{soln} is (in DMC) < (in PC) < (in water) for both Li–BF_4 and Li–PF_6. DMC is the most favorable solvent for CIP formation. According to ΔG^0_{soln} values calculated by eq 1, $LiBF_4$ has stronger tendency of forming CIP in all of the solvents examined than $LiPF_6$. $LiPF_6$ is harder to form a CIP, thus it is a better lithium salt for the electrolyte of the lithium second battery than $LiBF_4$ in this context.

4. CONCLUSION

The contact ion-pair (CIP) formation free energy of lithium ion with BF_4^- and PF_6^- in water, propylene carbonate (PC), and dimethyl carbonate (DMC) were calculated quantitatively by using the ER method combined with MD simulation. In vacuum the multidentate is more stable than the monodentate both for Li–BF_4 and Li–PF_6, while *the solvent effect* on monodentate is larger than multidentate in all solvents. Because *the solvent effect* of monodentate overwhelms energetic advantage of multidentate in vacuum, the monodentate CIP was more stable than the corresponding multidentate CIP in aqueous solutions. Likewise in carbonate solutions, monodentate Li–PF_6 CIP was more stable than tridentate Li–PF_6. On the other hand, no difference has been observed in free energy among Li–BF_4 mono- and bidentate CIP formations in carbonate solutions because of the compensation between the difference of *the solvent effect* in solution and the difference of ion-pair formation energy in vacuum. To investigate *the solvent effect* microscopic analyses of solute–solvent interaction were performed from energetic and structural viewpoints. Vacant sites of Li^+ cation in CIP are solvated with three carbonyl oxygen atoms of PC and DMC, and the solvation is stronger for the monodentate CIP than for the multidentate. Energetically favorable solute–solvent configurations are shown to be spatially more restricted for the multidentate CIP. For Li–PF_6 CIP, the Li–O distances in tridentate are slightly longer than in monodentate because of larger electrostatic repulsion. Eventually difference of solute–solvent interaction energy between mono- and tridentate Li–PF_6 CIPs is larger than that corresponding to the Li–BF_4 CIP. Therefore, monodentate was more stable than tridentate in carbonate solutions.

Although dielectric constant of PC is much larger than DMC's, the CIP formation free energies are almost same both in Li–BF_4 and Li–PF_6, thus the continuum model based on dielectric constant failed to explain such similar ion-pair formation behavior. Moreover, DMC conformational isomerism plays an important role in entropy as well as in enthalpy, when it solvates to the ions in solution. On the other hand, results obtained here are consistent with interpretation from the empirical solvent parameters derived from molecular features, e.g., the donor number (DN), the acceptor number (AN), and the $E_T(30)$ parameter. In this context, empirical interpretation of the CIP formation phenomena in electrolyte solutions for the lithium batteries were clarified and deepened at a molecular level quantitatively by solvation free energy calculations with the energy representation method combined with atomistic MD simulations.

AUTHOR INFORMATION

Present Address

[†]Graduate School of Science and Technology Niigata University, 8050, Ikarashi, 2-nocho, Nishi-ku, Niigata City, 950–2181, Japan

Notes

The authors declare no competing financial interest.

■ ACKNOWLEDGMENTS

N.M. is supported by the Grants-in-Aid for Scientific Research (Nos. 21300111 and 23651202) from the Japan Society for the Promotion of Science (JSPS), by the Grant-in-Aid for Scientific Research on Innovative Areas (No. 20118002) from the Ministry of Education, Culture, Sports, Science, and Technology of Japan, and by the Nanoscience Program and the Computational Materials Science Initiative of the Next-Generation Supercomputing Project. Y.U. is supported by the Grants-in-Aid for Scientific Research (Nos. 22P10750, 23350033 and 24655142) from the JSPS and by the Advanced Low Carbon Technology Research and Development Program (ALCA) from the Japan Science and Technology Agency (JST).

■ REFERENCES

(1) Ohtaki, H.; Radnai, T. *Chem. Rev.* **1993**, *93*, 1157.
(2) Ohtaki, H. *Monatsh. Chem.* **2001**, *132*, 1237.
(3) Ohtaki, H.; Ishiguro, S. *Complexation in Nonaqueous Solutions in Chemistry of Nonaqueous Solutions Current Progress*; Mamantov, G., Propov, A. I., Ed., VCH Publisher Inc.: Weinheim, Germany, 1994.
(4) Olsher, U.; Izatt, R. M.; Bradshaw, J. S.; Dalley., N. K. *Chem. Rev.* **1991**, *91*, 137.
(5) Marcus, Y. *Ion Solvation*: John Wiley & Sons Ltd: West Sussex, U.K., 1985.
(6) Smirnov, P. R.; Trostin, V. N. *Russ. J. Gen. Chem.* **2006**, *76*, 187.
(7) Chong, S.; Hirata, F. *J. Chem. Phys.* **1999**, *111*, 3654.
(8) Xu, K. *Chem. Rev.* **2004**, *104*, 4303.
(9) Tarascon, J.-M.; Armand, M. *Nature* **2001**, *414*, 359.
(10) Bohets, H.; van der Veken. *J. Phys. Chem. Chem. Phys.* **1999**, *1*, 1817.
(11) Soetens, J.-C.; Millot, C.; Maigret, B.; Bako, I. *Mol. Liq.* **2001**, *92*, 201.
(12) Papciak, R.; Mallory, V. *Acute Toxic.* **1990**, *1*, 15.
(13) Yamaguchi, T.; Hayakawa, M.; Matsuoka, T.; Koda, S. *J. Phys. Chem. B* **2009**, *113*, 11988.
(14) Yamaguchi, T.; Yamada, Y.; Matsuoka, T.; Koda, S.; Yasaka, Y.; Matubayasi, N. *J. Phys. Chem. B* **2011**, *115*, 12558.
(15) (a) Ue, M. *J. Electrochem. Soc.* **1994**, *141*, 3336. (b) Ue, M.; Mori, S. *J. Electrochem. Soc.* **1995**, *142*, 2577.
(16) (a) Hyodo, S.; Okabayashi, K. *Electrochim. Acta* **1989**, *34*, 1551. (b) Hyodo, S.; Okabayashi, K. *Electrochim. Acta* **1989**, *34*, 1557.
(17) (a) Battisti, D.; Nazri, G. A.; Klassen, B.; Aroca, R. *J. Phys. Chem.* **1993**, *97*, 5826. (b) Klassen, B.; Aroca, R.; Nazri, G. A. *J. Phys. Chem.* **1996**, *100*, 9334.
(18) (a) Cazzanelli, E.; Mustarelli, P.; Benevelli, F.; Appetecchi, G. B.; Croce, F. *Solid State Ionics* **1996**, *86−88*, 379. (b) Cazzanelli, E.; Croce, F.; Appetecchi, G. B.; Benevelli, F.; Mustarelli, P. *J. Chem. Phys.* **1997**, *107*, 5740.
(19) Barthel, J.; Buchner, R.; Wismeth, E. *J. Solution Chem.* **2000**, *29*, 937.
(20) Brooksby, P. A.; Fawcett, W. R. *Spectrochim. Acta A* **2006**, *64*, 372.
(21) Morita, M.; Asai, Y.; Yoshimoto, N.; Ishikawa, M. *J. Chem. Soc. Faraday Trans.* **1998**, *94*, 3451.
(22) Aroca, R.; Nazri, M.; Nazri, G. A.; Camargo, A. J.; Trsic, M. *J. Solution Chem.* **2000**, *29*, 1047.
(23) Doucey, L.; Revault, M.; Lautié, A.; Chaussé, A.; Messina, R. *Electrochim. Acta* **1999**, *44*, 2371.
(24) Burba, C. M.; Frech, R. *J. Phys. Chem. B* **2005**, *109*, 15161.
(25) (a) Hayamizu, K.; Aihara, Y.; Arai, S.; Martinez, C. G. *J. Phys. Chem. B* **1999**, *103*, 519. (b) Aihara, Y.; Sugimoto, K.; Price, W. S.; Hayamizu, K. *J. Chem. Phys.* **2000**, *113*, 1981.
(26) Kondo, K.; Sano, M.; Hiwara, A.; Omi, T.; Fujita, M.; Kuwae, A.; Iida, M.; Mogi, K.; Yokoyama, H. *J. Phys. Chem. B* **2000**, *104*, 5040.
(27) Tsunekawa, H.; Narumi, A.; Sano, M.; Hiwara, A.; Fujita, M.; Yokoyama, H. *J. Phys. Chem. B* **2003**, *107*, 10962.
(28) Kameda, Y.; Umebayashi, Y.; Takeuchi, M.; Wahab, M. A.; Fukuda, S.; Ishiguro, S.; Sasaki, M.; Amo, Y.; Usuki, T. *J. Phys. Chem. B* **2007**, *111*, 6104.
(29) Soetens, J.-C.; Millot, C.; Maigret, B. *J. Phys. Chem. A* **1998**, *102*, 1055.
(30) Tasaki, K. *J. Electrochem. Soc.* **2002**, *149*, A419.
(31) Áquist, J. *J. Phys. Chem.* **1990**, *94*, 8021.
(32) Leung, K.; Rempe, S. B.; Anatole von Lilienfeld, O. *J. Chem. Phys.* **2009**, *130*, 204507.
(33) Borodine, O.; Smith, G. D. *J. Phys. Chem. B* **2009**, *113*, 1763.
(34) Takeuchi, M.; Kameda, Y.; Umebayashi, Y.; Ogawa, S.; Sonoda, T.; Ishiguro, S.; Fujita, M.; Sano, M. *J. Mol. Liq.* **2009**, *148*, 99.
(35) Borodine, O.; Smith, G. D.; Jeffe, R. L. *J. Comput. Chem.* **2001**, *22*, 641.
(36) Mennuci, B.; Cancés, E.; Tomasi, J. *J. Phys. Chem. B* **1997**, *101*, 10506.
(37) Tomasi, J.; Persico, M. *Chem. Rev.* **1994**, *94*, 2027.
(38) Allen, M. P.; D. J. Tildesley, D. *J. Computer Simulation of Liquids*: Oxford University Press: Oxford, U.K., 1987.
(39) Matubayasi, N.; Nakahara, M. *J. Chem. Phys.* **2000**, *113*, 6070.
(40) Matubayasi, N.; Nakahara, M. *J. Chem. Phys.* **2002**, *117*, 3605; **2003**, *118*, 2446 (erratum)..
(41) Matubayasi, N.; Nakahara, M. *J. Chem. Phys.* **2003**, *119*, 9686.
(42) Karino, Y.; Fedorov, M. V.; Matubayasi, N. *J. Chem. Phys. Lett.* **2010**, *496*, 351.
(43) Matubayasi, N.; Liang, K. K.; Nakahara, M. *J. Chem. Phys.* **2006**, *124*, 154908.
(44) Matubayasi, N.; Shinoda, W.; Nakahara, M. *J. Chem. Phys.* **2008**, *128*, 195107.
(45) Takahashi, H.; Matubayasi, N.; Nakahara, M.; Nitta, T. *J. Chem. Phys.* **2004**, *121*, 3989.
(46) Rychaert, J. P. *J. Comput. Phys.* **1977**, *23*, 327.
(47) Berendsen, H. J. C.; Grigera, J. R.; Straatsma, T. P. *J. Phys. Chem.* **1996**, *100*, 1206.
(48) Gear, C. W. *Math. Comp.* **1967**, *21*, 146.
(49) Marcus, Y. *The Properties of Solvents: Wiley Series in Solutions Chemistry*: John Wiley & Sons Ltd: West Sussex, U.K., 1998.
(50) Hummer, G.; Pratt, L. R.; Garcia, A. E. *J. Phys. Chem.* **1996**, *100*, 1206.
(51) *Materials Explorer*; Fujitsu Limited: Tokyo, Japan, 2005.
(52) Marcus, Y. *Biophys. Chem.* **1994**, *51*, 111.
(53) Schmid, R.; Miah, A. M.; Sapunov, V. N. *Phys. Chem. Chem. Phys.* **2000**, *2*, 97.
(54) Tissadier, M. D.; Cowen, K. A.; Feng, W. Y.; Gundlach, E.; Cohen, M. H.; Earhart, A. D.; Coe, J. V. *J. Phys. Chem. A* **1998**, *102*, 7787.
(55) Jensen, K. P.; Jorgensen, W. L. *J. Chem. Theory Comput.* **2006**, *2*, 1499.
(56) Joung, I. S.; Cheatham, T. E., III. *J. Phys. Chem.* **2008**, *112*, 9020.
(57) Rempe, S. B.; Pratt, K. R.; Hummer, G.; Kress, J. D.; Martin, R. L.; Redondo, A. *J. Am. Chem. Soc.* **2000**, *122*, 966.
(58) Marcus, Y. *Pure Appl. Chem.* **1983**, *55*, 977.
(59) Takahashi, H.; Kawashima, Y.; Nitta, T.; Matubayasi, N. *J. Chem. Phys.* **2005**, *123*, 124504.
(60) Takahashi, H.; Takei, S.; Hori, T.; Nitta, T. *J. Mol. Struct. (THEOCHEM)* **2003**, *632*, 185.
(61) Hofmeister, F. *Arch. Exp. Pathol. Pharmakol. (Leipzig)* **1888**, *24*, 247. translated in Kunz, W.; Henle, J.; Ninham, B. W. *Curr. Opin. Colloid Interface Sci.* **2004**, *9*, 19.
(62) Frank, H. S.; Wen, W. Y. *Discuss. Faraday Soc.* **1957**, *44*, 133.
(63) Samoilov, O. Y. *Discuss. Faraday Soc.* **1957**, *44*, 141.
(64) Doucey, L.; Revault, M.; Lautié, A.; Chaussé., A.; Messina, R. *Electrochim. Acta* **1999**, *44*, 2371.
(65) Shannon, R. D. *Acta Crystallogr.* **1976**, *A32*, 751.
(66) Gutmann, V. *Coord. Chem. Rev.* **1967**, *2*, 239.
(67) Reichardt, C. *Chem. Rev.* **1994**, *94*, 2319.